Analysis of the behaviour of limestone sorbents for sorption-enhanced gasification in dual interconnected fluidised bed reactor

Antonio Coppola [a], Fiorella Massa [b], Fabio Montagnaro [c,*], Fabrizio Scala [b,a]

[a] *Institute of Sciences and Technologies for Sustainable Energy and Mobility (STEMS), National Research Council (CNR), Piazzale Vincenzo Tecchio 80, 80125 Naples, Italy*
[b] *Department of Chemical, Materials and Industrial Production Engineering, University of Naples Federico II, Piazzale Vincenzo Tecchio 80, 80125 Naples, Italy*
[c] *Department of Chemical Sciences, University of Naples Federico II, Complesso Universitario di Monte Sant'Angelo, 80126 Naples, Italy*

ABSTRACT

Sorption-Enhanced Gasification (SEG) is a promising technology based on the use of Ca-based sorbents (like limestone) to selectively remove CO$_2$ from the gasification environment, for production of hydrogen rich syngas. This process benefits from the extensive understanding of "calcium looping", a post-combustion technique aimed at removing CO$_2$ from flue gas. Calcium looping is most typically carried out in Dual Interconnected Fluidised Bed (DIFB) reactors. The correct design of sorbent looping processes in DIFB reactors must consider: 1) sorbent deactivation (i.e., decay of CO$_2$ capture performance) over repeated cycling; 2) the loss of sorbent material due to elutriation, that may be enhanced by attrition and fragmentation. The aim of this study is to investigate six different commercial limestones in terms of sorbent performance and attrition/fragmentation tendency under simulated SEG conditions.

The experimental campaign was carried out in a lab-scale DIFB reactor, electrically heated. The six sorbents were limestones coming from different parts of Europe. A synthetic gas including air, CO$_2$ and N$_2$ was used to simulate SEG conditions. A "test" consisted of ten complete cycles of calcination/carbonation. Calcination was performed at 850 °C, fluidising the bed with a stream of 10 % CO$_2$ (balance air) to simulate oxidising conditions typical of the combustor-calciner. In the carbonation stage, the temperature was kept at 650 °C and the CO$_2$ concentration was set at 10 % (balance nitrogen) to account for reducing conditions typical of the gasifier-carbonator.

During each carbonation stage, the CO$_2$ concentration at the exhaust was continuously monitored to calculate the CO$_2$ specific capture performance. The sorbent attrition rate was determined by working out the mass of fines elutriated at the exhaust and collected in filters, for each calcination and carbonation stage. After a test, each exhaust sorbent sample was sieve-analysed to obtain the particle size distribution and the fraction of generated fragments. Moreover, the characterisation was extended by carrying out, in an *ex situ* apparatus, impact fragmentation tests on samples preprocessed in DIFB.

Results were critically analysed in the light of the adopted operating conditions, by also including: (a) a fitting equation of conversion data, able to give indications on the sorbent resistance to sintering; (b) a carbonation reaction model, that allowed the estimation of the decrease in the sorbent specific surface area as long as the number of cycles increases.

1. General overview

Sorption-Enhanced Gasification (SEG) can rely on the use of inexpensive Ca-based sorbent (like limestone) for CO$_2$ removal from syngas *in situ* during gasification of a solid fuel. CO$_2$ capture pushes the equilibrium of the water–gas shift reaction towards the products, and this allows the production of syngas rich in H$_2$ [1]. This process resembles, though with specific differences, Calcium Looping (CaL), a post-combustion technique aimed at removing CO$_2$ from flue gas. Calcium looping is usually carried out in a Dual Interconnected Fluidised Beds (DIFB) reactor arrangement, with the Ca-based sorbent being cycled between the carbonator, where CO$_2$ capture from flue gas takes place,

* Corresponding author.
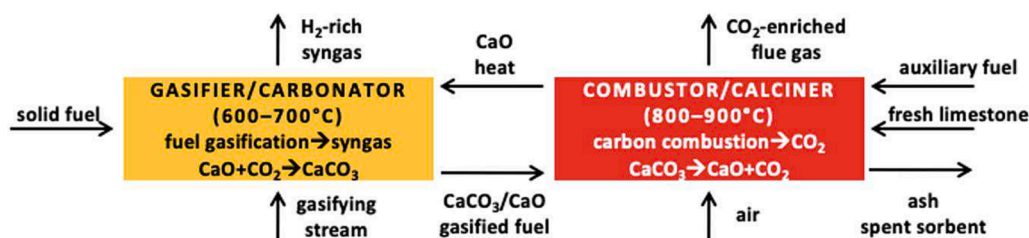*E-mail address:* fabio.montagnaro@unina.it (F. Montagnaro).

Fig. 1. Scheme for sorption-enhanced gasification of a solid fuel in dual interconnected fluidised beds.
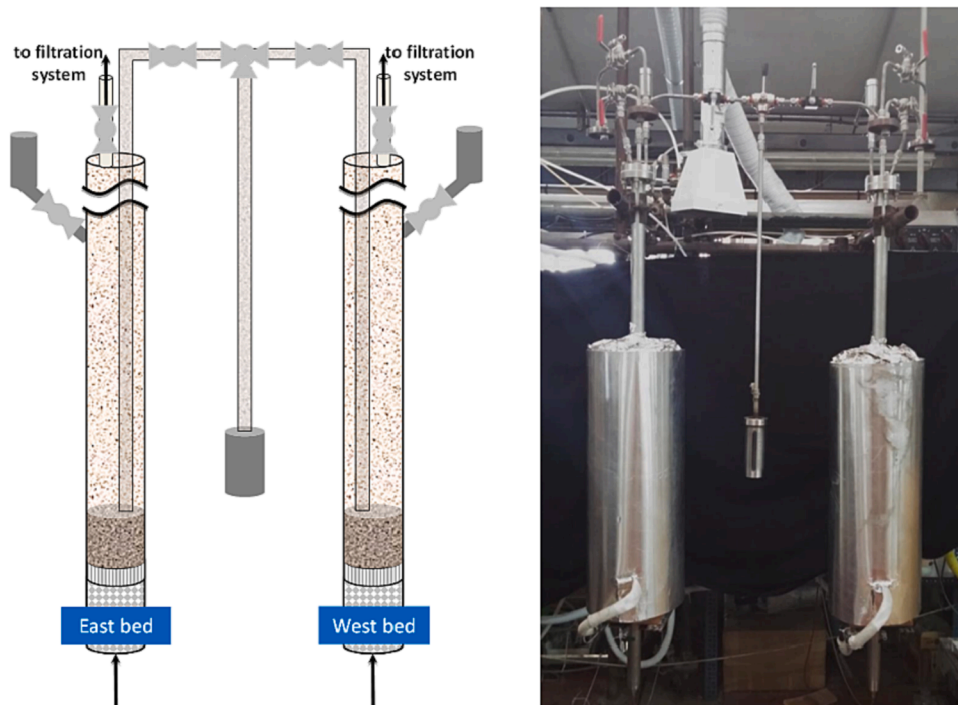

Fig. 2. "Twin Bed" DIFB reactor used in the experimental campaign.

Table 1
Main operating conditions for simulated SEG tests, and purity level in $CaCO_3$ for the six parent limestones.

Stage	T, °C	Duration, min	%vol. CO_2 (balance)	Fluidisation velocity, m/s
Calcination	850	10	10 (air)	0.5
Carbonation	650	10	10 (N_2)	0.5
Sorbent			f_{CaCO_3} [-]	
MAS			0.974	
SAR			0.985	
TAR			0.965	
CZA			0.944	
SCH			0.958	
EBW			1	

and the calciner, where the sorbent discharges a stream of concentrated CO_2 (ready for further processing, and then use/storage) and it is restored for another cycle [2–10].

The process scheme is exemplified in Fig. 1. Solid fuel is fed to the gasifier-carbonator, along with the gasifying stream. Gasification occurs at circa 600–700 °C, yielding a primary syngas. The reactor is also fed with a stream of CaO: the capture of CO_2 from the primary syngas takes place via CaO carbonation (CaO + CO_2→$CaCO_3$), giving: (i) a secondary syngas rich in H_2 (and depleted in CO_2); (ii) a solid stream (carbonated sorbent comprising unconverted CaO + solid char gasified and with residual carbon). This stream is sent to the combustor-calciner, operated at 800–900 °C, where it is contacted with air and, in case of need, extra fuel. In this reactor the sorbent is regenerated following calcination ($CaCO_3$→CaO + CO_2), to produce a CaO stream ready for a new cycle. The operation of the calciner must consider that: (i) this reactor operates at higher temperature than the carbonator, and limestone calcination is endothermic; (ii) the stream of regenerated sorbent acts as heat carrier, so to support the conditions in the gasifier-carbonator, as gasification reactions are overall endothermic.

The correct design of sorbent looping processes in DIFB reactors must reflect the following issues: (i) sorbent deactivation (i.e., decay of CO_2 capture performance) during continuous cycling operations, due to thermal and chemical sintering; (ii) loss of sorbent material due to elutriation, boosted by attrition and fragmentation [11]. Occurrence of (i) and (ii) obliges to a continuous make-up of raw (fresh) sorbent to counterweigh losses of sorbent uptake performance: a "chemical" loss due to sintering, and a "physical" loss due to elutriation.

In literature, detailed information on gasifier performance, reactor design and process analysis when a Ca-based sorbent is used for SEG of a solid fuel is reported, both in fluidised bed [12–18] and other types of reactors [19–22]. Further review papers on the subject can be found at Refs. [23–25]. On the other hand, the emphasis on the role that the operational conditions for a SEG process based on CaL have on the CO_2
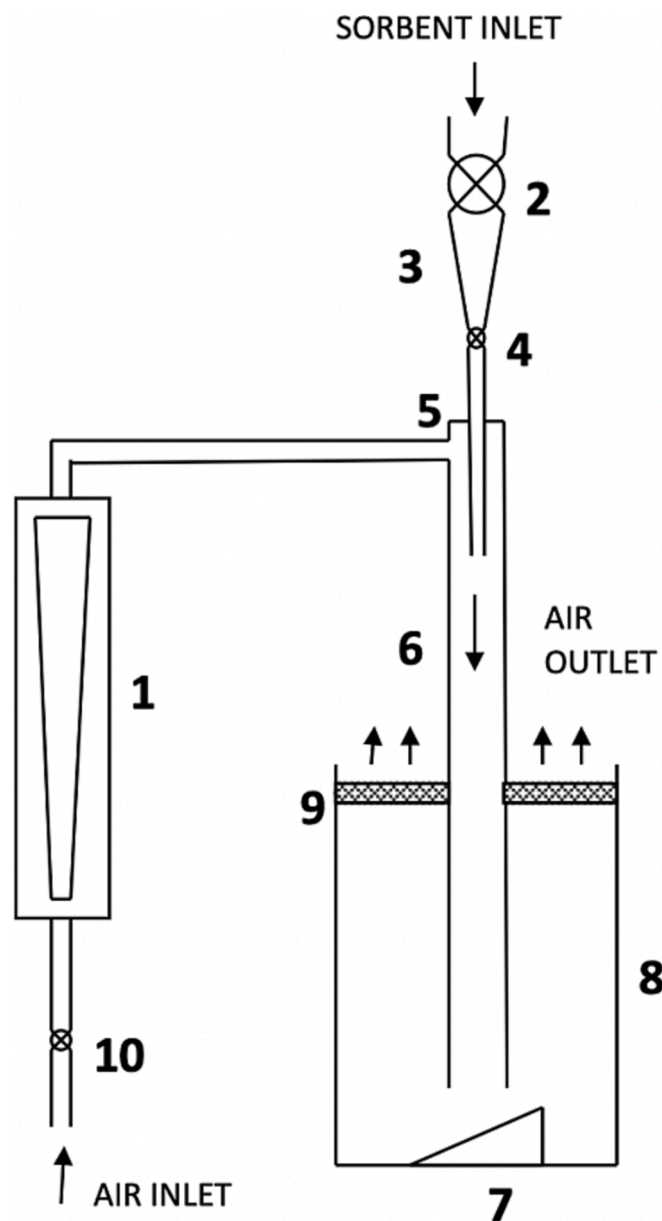
Fig. 3. *Ex situ* impact fragmentation apparatus (1 = gas flowmeter; 2 and 4 = lock hopper valves; 3 = hopper; 5 = feeding tube; 6 = eductor tube; 7 = target plate; 8 = collection chamber; 9 = cellulose filter; 10 = gas flow metering valve).

capture ability of the sorbent, and its attrition propensity, still merits attention.

In this framework, following a previous manuscript which focused on one reference limestone and on the role of steam in the system [26], our present contribution is to analyse the CO_2 uptake performance and attrition/fragmentation tendency (when operating conditions simulating those of a DIFB-SEG process are adopted) for six commercial limestones in a lab-scale DIFB reactor, by voluntarily excluding the effect of the solid fuel. Additionally, the tendency to undergo impact fragmentation (able to influence, through changes in particle size, their reactivity and elutriation tendency) for sorbent particles under DIFB-SEG conditions is a subject hardly tackled. Therefore, another element of novelty was represented by carrying out experiments in an *ex situ* impact test rig, by characterising the behaviour of DIFB-SEG pre-processed samples.
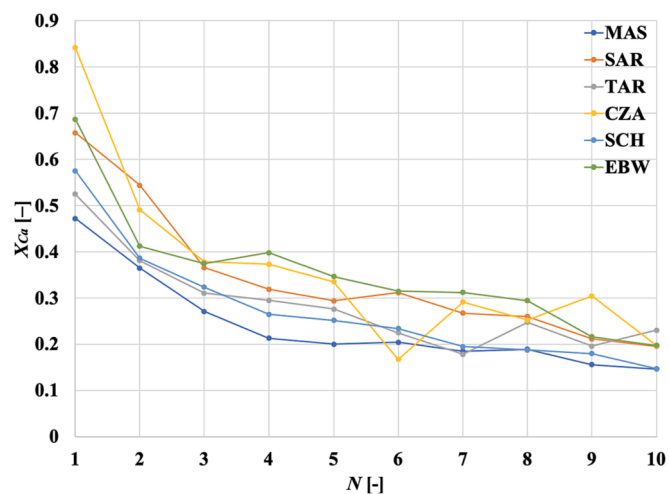

Fig. 4. Degree of Ca conversion (Eq. (1)) as a function of *N*, the number of carbonation stages, for DIFB-SEG tests (six different limestones).

2. Experimental section

2.1. Tests in dual interconnected fluidised bed system

A purposely designed DIFB system (lab-scale), named Twin Bed (TB), served for SEG tests. The TB installation (Fig. 2) is made by two identical fluidised beds, operated in bubbling regime, electrically heated (inner diameter = 40 mm), acting as calciner and carbonator, respectively. The two reactors are connected each other by a duct (inner diameter = 10 mm) partly dipped into the dense zone of the beds, which allows the pneumatic transport of the solid bed from one reactor to the other. The two reactors are autonomously operated batchwise with respect to the solid particles. Valves permit to regulate the transfer of solid streams between the two reactors. At the outlet of each reactor, gas is transferred to sintered steel filters (capture efficiency > 99 % for > 10 μm particles) for collection of elutriated fines. The reader is referred to the works by Coppola et al. [27,28] for more details on the DIFB apparatus.

The sorbents used in the investigation were 6 different natural limestones coming from different parts of Europe, all of them with an elevated content of $CaCO_3$ (94–100 %wt.): two from Italy, named Massicci (MAS; Tuscany region) and Sardo (SAR; Sardinia region), respectively; two from Poland, named Tarnów Opolski (TAR; Lesser Poland region) and Czatkowice (CZA; Lower Silesian region), respectively; and two from Germany (Baden-Württemberg region), i.e., Schwabian Alb (SCH) and EnBW (EBW), respectively.

Table 1 lists the main operating conditions for DIFB-SEG tests. Cylinders of CO_2 and N_2, with a flow meter/controller, were used to make surrogate flue gases aiming at reproducing SEG conditions. The test, on each single sorbent, comprised ten complete cycles of calcination/ carbonation, plus an eleventh calcination stage (resulting in 21 total stages). The initial mass of limestone sorbent was $m_0 = 10$ g, sieved in the size range 400–600 μm. Silica sand (size 850–1000 μm) was put in both reactors as fluidisation/thermal ballast material. At the beginning of each test, the sorbent was fed to the calciner: the calcination stage was executed at $T = 850$ °C fluidising the bed with a stream of 10 % (by volume) CO_2 (balance air), to simulate oxidising conditions of the combustor-calciner (Fig. 1). For the carbonation stage, the temperature was kept at 650 °C and the CO_2 concentration was set at 10 % by volume, balanced by nitrogen, to simulate reducing conditions typical of the gasifier-carbonator (Fig. 1). Each stage lasted for 10 min. Both beds were fluidised at a superficial velocity of 0.5 m/s, at process conditions, i.e., twice the sand minimum fluidisation velocity.

The CO_2 concentration in the gas stream exiting from the carbonator was continuously examined by a NDIR analyser. This allowed to express
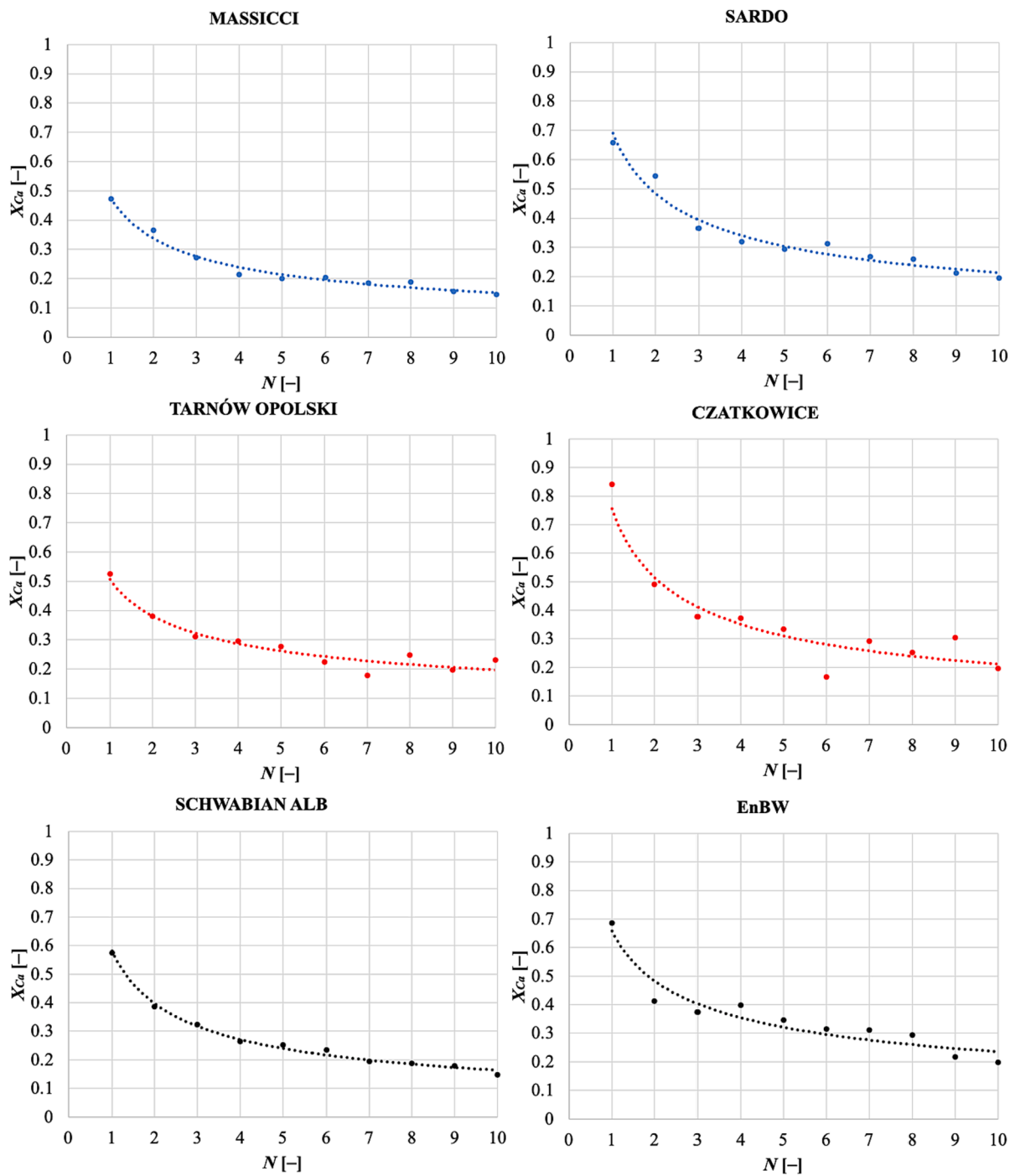
Fig. 5. Fitting of $X_{Ca}(N)$ data according to the IAD Eq. (5) proposed in this work (six different limestones).

Table 2
Values for the decay constant (IAD model) for the six cases under investigation.

Sorbent			k_2 [–]	R^2 [–]
MAS			0.497	0.9775
SAR			0.510	0.9587
TAR			0.410	0.9401
CZA			0.552	0.9148
SCH			0.551	0.9934
EBW			0.447	0.9142

the carbonation degree of Ca (the moles of Ca cumulatively reacted to CaCO$_3$ in a carbonation stage, divided by the moles of Ca initially charged in the DIFB system) as:

$$X_{Ca} = \frac{\int_0^t \left[W_{CO_2}^{in} - W_{CO_2}^{out}(t) \right] dt}{m_0 f_{CaCO_3}} \frac{MW_{CaCO_3}}{MW_{CO_2}} \tag{1}$$

where $W_{CO_2}^{in}$ indicates the mass flow rate of CO_2 at the carbonator inlet, $W_{CO_2}^{out}(t)$ is the mass flow rate of CO_2 at its outlet, t is the carbonation time, MW is the molecular weight and f_{CaCO_3} is the mass fraction of CaCO$_3$ in the parent limestone (i.e., its purity in CaCO$_3$), whose values have been listed in Table 1.
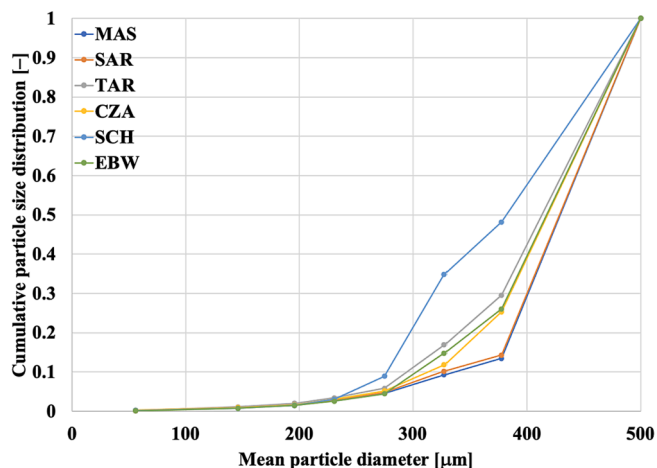
Fig. 6. Cumulative size distribution for in-bed sorbent particles retrieved at the end of simulated DIFB-SEG tests (six different limestones).

Table 3

Values for the cumulative mass fraction of fragments for in-bed sorbent particles retrieved at the end of simulated DIFB-SEG tests (Eq. (3)), and for the specific elutriation rate averaged over the 21 stages of simulated DIFB-SEG tests, Eq. (2) (six different limestones).

	MAS	SAR	TAR	CZA	SCH	EBW
f_{FR}^{in-bed} [–]	0.134	0.143	0.296	0.253	0.482	0.260
E_{av} [mg/(g min)]	0.0142	0.0144	0.0173	0.0120	0.0133	0.0119

The sorbent attrition rate for each stage (calcination or carbonation) was calculated by weighting the mass of fines elutriated and gathered in the filters. The specific elutriation rate E is expressed as the mass of sorbent fines cumulatively collected over a stage, m_{el}, divided by the initial sorbent mass and by the duration of the stage, Δt (10 min):

$$E = \frac{m_{el}}{m_0 \Delta t} \tag{2}$$

The Particle Size Distribution (PSD) of the sorbent was characterised by sieving the bed material at the end of the test (21 stages). Sieving was performed in 9 particle size ranges, with mean diameter d_i equal to, respectively, 56, 146, 196, 231, 275, 327.5, 377.5 and 500 µm. We defined $x(d_i)$ the mass fraction of particles falling in a size interval with mean diameter d_i, and we considered as "fragments" the particles finer than the lower limit of the parent particle size range (400–600 µm). Therefore, the cumulative mass fraction of in-bed fragments reads:

$$f_{FR}^{in-bed} = \sum_{d_i < 400\mu m} [x(d_i)] \tag{3}$$

After the DIFB-SEG test, sorbent particles were subjected to *ex situ* impact fragmentation experiments, as described in the following.

2.2. Impact fragmentation tests

When sorbent particles are treated in full-scale fluidised beds, they undergo fragmentation by impact damage, following high-velocity collisions between particles and targets (bed internals or other bed solids) [26,29,30]. Depending on the extent and pattern of impact fragmentation, coarse (non elutriable) and fine (elutriable) fragments can be obtained. Scale and fluid-dynamics of our lab-scale DIFB reactor do not encourage impact fragmentation conditions; therefore, the phenomenon was scrutinised in an *ex situ* apparatus, operated at room temperature and depicted in Fig. 3. It relies on the concept of entraining particles in a gas stream at controlled velocity and impacting them against a solid target. The system is based on a vertical stainless steel eductor tube, 1 m high, inner diameter = 10 mm, equipped with a stainless steel particle feed hopper. A measured air flow enters the top section of the eductor. The sorbent particles in the hopper are transported through the tube, and they are accelerated by the air flow. At the eductor tube exit,

Table 4

Values for sorbent specific surface area (Eq. (8)) expressed in m²/g as a function of the carbonation stage (six different limestones). The last row reports the loss in specific surface area after ten carbonation stages vs the value calculated after the first carbonation stage.

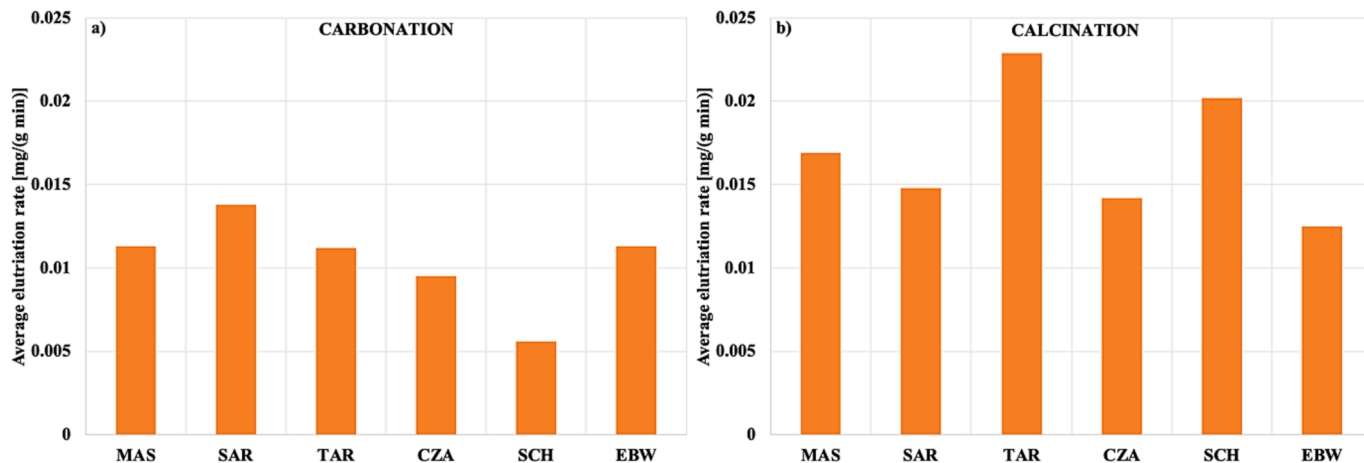| N	MAS	SAR	TAR	CZA	SCH	EBW
1	2.105	2.526	3.228	3.508	2.807	3.368
2	1.263	1.123	2.807	1.684	1.965	1.544
3	0.982	1.123	2.807	1.123	1.263	1.263
4	0.982	0.982	2.526	1.965	0.982	2.526
5	0.702	0.982	2.386	1.544	0.982	0.842
6	0.702	0.842	1.965	1.965	1.123	1.123
7	0.702	0.842	1.403	0.702	0.982	0.982
8	0.702	0.702	2.526	0.702	0.842	0.842
9	0.561	0.702	0.842	0.702	0.842	0.702
10	0.561	0.702	0.982	0.421	0.561	0.561
Loss, %	73.35	72.21	69.58	88.00	80.01	83.34

Fig. 7. Average value for the specific elutriation rate, expressed as mg of elutriated fines per minute and per g of initial sorbent, over a) the 10 carbonation and b) 11 calcination stages, for the six sorbents under scrutiny.
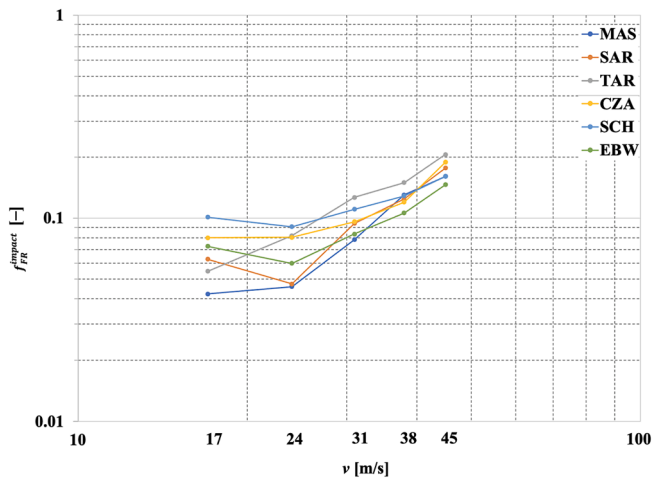
Fig. 8. Cumulative mass fraction of fragments generated upon impact vs impact velocity for the six materials after pre-processing in the DIFB system. Log–log chart.
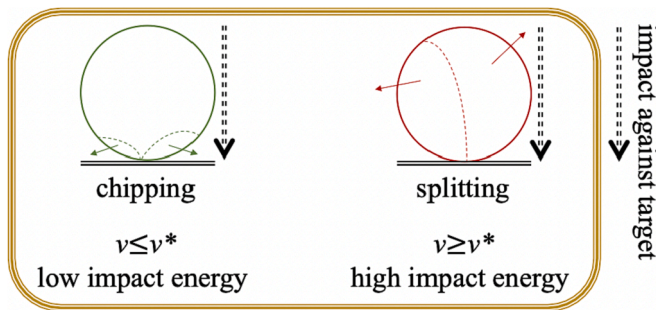

Fig. 9. Chipping/splitting transition at increasing impact velocity against a solid target for semi brittle materials. Dashed lines represent the propagation of fractures.

particles impact on the target placed in a glass collection chamber 50 mm below the bottom end of the tube. The target is made of stainless steel and is inclined by 30° with respect to the horizontal. The particle impact velocity v is calculated as the sum of the gas velocity in the eductor and the particle terminal velocity [29]. After the impact, the debris is collected for PSD analysis. Full description of the system can be found in our previous paper [26].

At the end of a complete DIFB-SEG test a mass of 1 g of each of the six sorbents was subjected to impact fragmentation tests, after re-sieving in the reference 0.4–0.6 mm size interval. Values of v were: 17, 24, 31, 38 and 45 m/s, chosen to represent typical conditions in FB reactors. PSD of the impacted particles was calculated as previously described for in-bed sorbent fragments. Similarly to Eq. (3), it was defined f_{FR}^{impact}, the cumulative mass fraction of impacted fragments. For each of the six sorbents, f_{FR}^{impact} can be reported as a function of v. Plotting $f_{FR}^{impact}(v)$ on a log–log chart allows to underline the establishment of power-law relationships, on the type of $f_{FR}^{impact} \propto v^k$. Moreover, PSD data have been converted into Probability Density Functions (PDF) of impacted particles:

$$\text{PDF}(d_i) = \frac{x(d_i)}{w(d_i)} \tag{4}$$

i.e., the ratio, for a given size interval having width $w(d_i)$, between $x(d_i)$ obtained from PSD and the width itself.

3. Results and discussion

3.1. Degree of Ca conversion for sorbents in simulated DIFB-SEG tests

Fig. 4 reports the values for X_{Ca} vs the number N of carbonation stages for the simulated DIFB-SEG tests carried out with the six different sorbents. The effect of thermal sintering is evident from the decline of X_{Ca} upon iterated calcination/carbonation cycles. The decay is more pronounced after the first cycles, to slow down thereafter. For $N = 1$, X_{Ca} ranges from 84.1 % (for the sorbent with highest initial reactivity, i.e., CZA) to 47.2 % (for the sorbent with lowest initial reactivity, i.e., MAS). For $N = 10$, X_{Ca} ranges in a narrower interval, i.e., from 23.0 % (for the sorbent with highest long-term reactivity, i.e., TAR) to 14.6–14.7 % (for the sorbents with lowest long-term reactivity, i.e., MAS and SCH). Averaging (suffix "av") the values for X_{Ca} over the 10 carbonation stages, we found:

o Sorbents CZA ($X_{Ca,av} = 36.3$ %), EBW ($X_{Ca,av} = 35.5$ %) and SAR ($X_{Ca,av} = 34.3$ %) with fairly good capture capacity, i.e., a mean carbonation degree around 1/3;
o Sorbents TAR ($X_{Ca,av} = 28.6$ %), SCH ($X_{Ca,av} = 27.4$ %) and MAS ($X_{Ca,av} = 24.0$ %) with lower capture capacity.

Post-processing of $X_{Ca}(N)$ data has been carried out by postulating here the following IAD "Initial Activity Decay" equation:

$$X_{Ca}(N) = k_1 N^{-k_2} \tag{5}$$

where k_1 is the initial activity constant, that measures the capacity of the sorbent when $N = 1$ ($X_{Ca}(N = 1) = k_1$), and k_2 is the decay constant that takes into account the resistance of the sorbent to sintering phenomena which cause decrease its performance (the higher k_2, the worst the sintering resistance). While Fig. 5 shows data fitting with the IAD Eq. (5), Table 2 lists the best-fitting values for k_2 (along with the values for the coefficient of determination). TAR and EBW sorbents showed the best resistance to deactivation with increasing number of cycles, while SCH and CZA the worst one.

3.2. In-bed sorbents attrition/fragmentation

Fig. 6 illustrates the cumulative PSD for each sorbent sample at the end of the simulated DIFB-SEG tests. The values for the cumulative mass fraction of in-bed fragments, Eq. (3), are correspondingly listed in Table 3:

o Sorbent SCH ($f_{FR}^{in-bed} = 48.2$ %) is the one more prone to undergo in-bed particle fragmentation;
o TAR, EBW and CZA have intermediate behaviour in this respect, with f_{FR}^{in-bed} ranging from 25.3 % and 29.6 %;
o SAR and MAS are the sorbents showing a more limited production of fragments, whose cumulative mass fraction results, after 21 stages, in the range 13–14 %.

The specific elutriation rate, Eq. (2), was determined from the amount of sorbent collected at the exhaust during calcination and carbonation stages. In Fig. 7a and 7b, we report the average value for E over the 10 carbonation stages and the 11 calcination stages, respectively, for the six sorbents under scrutiny. In Table 3, the average value for E (over the 21 stages of each test), for the six investigated sorbents, is listed. It lies in the range 0.0119–0.0173 mg/(g min), corresponding to an average fractional loss of sorbent, per stage, in the range 0.0119–0.0173 % with respect to the initial mass of sorbent (each stage lasted 10 min). It is observed that, during calcination (average values for E in the range 0.0125–0.0229 mg/(g min)), the production of fines is more pronounced, an aspect likely related to the higher thermal stresses induced on the sorbent particles by the higher operating temperature vs
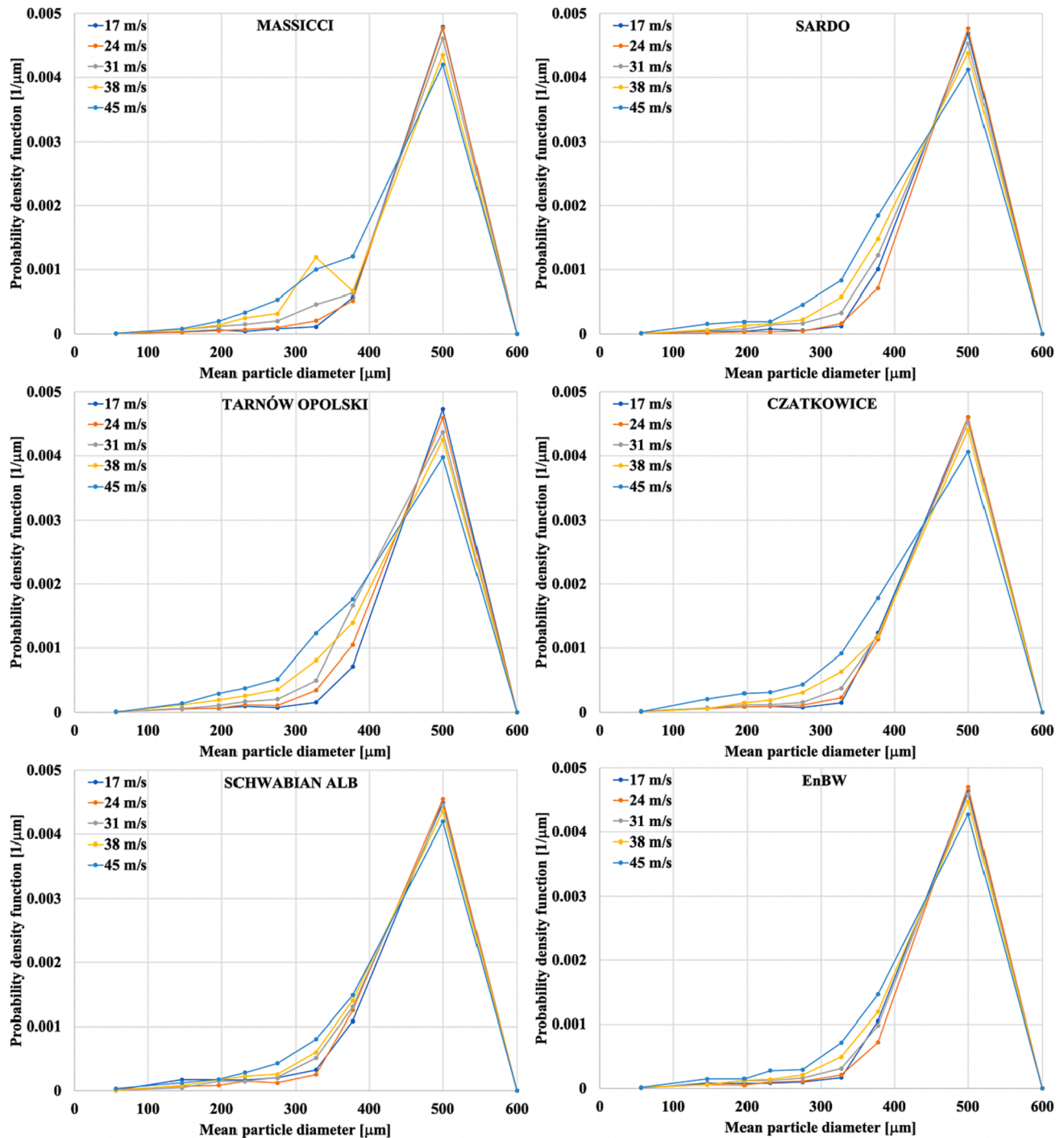
Fig. 10. Probability density functions, Eq. (4), of particle size for debris collected after impact fragmentation tests for the six materials after pre-processing in the DIFB system. Impact velocity is reported in legend.

carbonation (average values for E in the range 0.0056–0.0138 mg/(g min)). In addition, it has to be recalled that carbonation of CaO increases the mechanical strength of the particle (as $CaCO_3$ is harder than CaO), thus contributing to improve the resistance to surface abrasion upon carbonation stages.

3.3. Carbonation reaction model and evaluation of sorbent specific surface area

According to the work by Grace and colleagues [31], for carbonation kinetics having zero order, the reaction rate at time zero:

$$r_0 = \frac{1}{3} \frac{dX_{Ca}}{dt}\bigg|_{t=0} \tag{6}$$

can be expressed as:

$$\ln(r_0) = \ln\left(\frac{56 k_0 S_0}{3}\right) - \frac{E_a}{RT} \tag{7}$$

where E_a is the carbonation reaction activation energy (29 kJ/mol), k_0 is the pre-exponential factor of the carbonation kinetic constant (1.67×10^{-3} mol/(m^2 s)) and S_0 the initial sorbent specific surface area,

expressed in [m²/g]. By working out the time-series values of the exit CO_2 concentration during each of the 10 carbonation stages, one obtains the $X_{Ca}(t)$ profiles and, thus, the values for r_0 referring to each carbonation stage. Then, by manipulation of Eq. (7):

$$S_0 = \frac{3}{56k_0} \exp\left[\ln(r_0) + \frac{E_a}{RT}\right]$$ (8)

one gets how S_0 varies along with the carbonation cycles, for each sorbent. Values are listed in Table 4. While S_0, for $N = 1$, ranges from 2.1 m²/g (MAS) to 3.5 m²/g (CZA), it steadily decreases down to the range 0.42–0.98 m²/g when $N = 10$, to confirm the effect that thermal sintering (determining a loss in $S_0(N = 10)$ vs $S_0(N = 1)$ from 70 % to 88 % depending on the sorbent) has in reducing the sorbent surface area available for CO_2 capture.

3.4. Impact fragmentation tendency

Fig. 8 reports log–log $f_{FR}^{impact}(v)$ plots for the five values of impact velocity scrutinised, for each of the six sorbents pre-processed in the DIFB system under simulated SEG conditions. As a general trend, obviously, the fraction of fragments generated by impact increases as the impact velocity increases. As already discussed in our previous works [29,30], for low impact velocity (i.e., low impact energy) the transmission of fractures upon impact is mainly restricted at the particles surface, so predominantly generating fine chips (that can be perceived as fragments of size much finer than the parent particle size). We call "chipping" this impact fragmentation pattern. When the energy associated to impact rises, the fractures can propagate throughout the particle, ending up into the "splitting" of the parent particles into fragments of comparable size. Splitting determines a more significant mass production of fragments. This chipping/splitting pattern can be applied to semi brittle materials, as the case for a sorbent sample pre-processed (and, partly sintered) for many cycles during DIFB-SEG operation. The transition from chipping to splitting can be observed by a change in slope in $f_{FR}^{impact}(v)$ curves when a critical impact velocity v^* is reached. Fig. 9 schematically depicts this scenario.

At the lowest impact velocity investigated, $v = 17$ m/s, f_{FR}^{impact} is in the range 4.2 % (MAS)–10.1 % (SCH). At the highest value of v (45 m/s), f_{FR}^{impact} falls between 14.6 % (EBW) and 20.6 % (TAR). Apart from some scatter of data, for all the sorbents but TAR the critical velocity where we observed a change in slope (transition from chipping to splitting) is v^*=24 m/s. Further insights can be gained by the inspection of PDF curves in Fig. 10. For all sorbents, when the impact velocity increases from 17 m/s up to 45 m/s, the PDF curves progressively increase their value corresponding to finer particles, in line with the more extended generation of fragments when the energy associated with the impact event is higher.

4. Concluding remarks

The characterisation of the six sorbents presented in this research article shows that, despite the similar chemical composition, they behave differently in terms of CO_2 capture performance, resistance to sintering and production of both fragments and elutriable fines, under operating conditions resembling DIFB-SEG. Furthermore, a specifically devoted *ex situ* investigation showed that the materials, pre-processed in DIFB, underwent impact fragmentation following a chipping/splitting pattern as a function of the increase in the impact velocity. Results presented here can be useful for the determination of the make-up of fresh sorbent required for steady operation and for optimal design and operation of sorption-enhanced gasification, as they give indication on CO_2 capture performance and loss of material by attrition/fragmentation. On the basis of the present results, such loss is predicted to be relatively limited under DIFB-SEG conditions, so that the sorbent make-

up rate would be most likely determined by the need to compensate the decline of CO_2 capture capacity due to sintering.

CRediT authorship contribution statement

Antonio Coppola: Conceptualization, Data curation, Investigation, Methodology, Software, Supervision, Validation. **Fiorella Massa:** Data curation, Investigation, Methodology. **Fabio Montagnaro:** Conceptualization, Data curation, Formal analysis, Project administration, Software, Supervision, Validation, Visualization, Writing – original draft. **Fabrizio Scala:** Conceptualization, Funding acquisition, Project administration, Resources, Supervision, Validation.

Declaration of Competing Interest

The authors declare that they have no known competing financial interests or personal relationships that could have appeared to influence the work reported in this paper.

Data availability

Data will be made available on request.

Acknowledgements

References

[1] Florin NH, Harris AT. Enhanced hydrogen production from biomass with in situ carbon dioxide capture using calcium oxide sorbents. Chem Eng Sci 2008;63: 287–316.

[2] Rodríguez N, Alonso M, Abanades JC. Experimental investigation of a circulating fluidized-bed reactor to capture CO_2 with CaO. AIChE J 2011;57:1356–66.

[3] Erans M, Manovic V, Anthony EJ. Calcium looping sorbents for CO_2 capture. Appl Energy 2016;180:722–42.

[4] Perejón A, Romeo LM, Lara Y, Lisbona P, Martínez A, Valverde JM. The calcium-looping technology for CO_2 capture: on the important roles of energy integration and sorbent behaviour. Appl Energy 2016;162:787–807.

[5] Coppola A, Senneca O, Scala F, Montagnaro F, Salatino P. Looping cycles for low carbon technologies: a survey of recent research activities in Naples. Fuel 2020; 268:117371.

[6] Liu C, Lin Q, Han Y, Wu S. High-temperature attrition of nano CaO-based CO_2-reactive adsorbents in the calcium looping process. Ind Eng Chem Res 2020;59: 16052–8.

[7] Chen L, Dai W, Wang C, Wang W, Anthony EJ. The combined effect of SO_2 and H_2O on CO_2 capture performance by calcium looping. J CO_2 Util 2021;54:101798.

[8] Dunstan MT, Donat F, Bork AH, Grey CP, Müller CR. CO_2 capture at medium to high temperature using solid oxide-based sorbents: fundamental aspects, mechanistic insights, and recent advances. Chem Rev 2021;121:12681–745.

[9] Moreno J, Homsy SL, Schmid M, Scheffknecht G. Calcium looping: sorbent and process characterization in a 20 kW$_{th}$ dual fluidized bed. Energy Fuels 2021;35: 16693–704.

[10] Arcenegui Troya JJ, Moreno V, Sanchez-Jiménez PE, Perejón A, Valverde JM, Pérez-Maqueda LA. Effect of steam injection during carbonation on the multicyclic performance of limestone ($CaCO_3$) under different calcium looping conditions: a comparative study. ACS Sustain Chem Eng 2022;10:850–9.

[11] Coppola A, Esposito A, Montagnaro F, Iuliano M, Scala F, Salatino P. The combined effect of H_2O and SO_2 on CO_2 uptake and sorbent attrition during fluidised bed calcium looping. Proc Comb Inst 2019;37:4379–87.

[12] Pitkäoja A, Ritvanen J, Hafner S, Hyppänen T, Scheffknecht G. Simulation of a sorbent enhanced gasification pilot reactor and validation of reactor model. Energ Conver Manage 2020;204:112318.

[13] Ma X, Li Y, Huang X, Feng T, Mu M. Sorption-enhanced reaction process using advanced Ca-based sorbents for low-carbon hydrogen production. Process Saf Environ Prot 2021;155:325–42.

[14] Parvez AM, Hafner S, Hornberger M, Schmid M, Scheffknecht G. Sorption enhanced gasification (SEG) of biomass for tailored syngas production with in-situ CO_2 capture: current status, process scale-up experiences and outlook. Renew Sust Energy Rev 2021;141:110756.

[15] Dai J, Whitty KJ. Chemical looping gasification and sorption enhanced gasification of biomass: a perspective. Chem Eng Process 2022;174:108902.

[16] Liu G, Zhao Y, Heberlein S, Veksha A, Giannis A, Chan WP, et al. Hydrogen and power co-production from autothermal biomass sorption enhanced chemical

looping gasification: thermodynamic modeling and comparative study. Energ Conver Manage 2022;269:116087.

[17] Martínez I, Callén MS, Grasa G, López JM, Murillo R. Sorption-enhanced gasification (SEG) of agroforestry residues: influence of feedstock and main operating variables on product gas quality. Fuel Process Technol 2022;226: 107074.

[18] Žalec D, Hanak DP, Može M, Golobič I. Process development and performance assessment of flexible calcium looping biomass gasification for production of renewable gas with adjustable composition. Int J Energy Res 2022;46:6197–215.

[19] Chen S, Zhao Z, Soomro A, Ma S, Wu M, Sun Z, et al. Hydrogen-rich syngas production via sorption-enhanced steam gasification of sewage sludge. Biomass Bioenerg 2020;138:105607.

[20] Di Giuliano A, Gallucci K, Foscolo PU. Determination of kinetic and diffusion parameters needed to predict the behaviour of CaO-based CO_2 sorbent and sorbent-catalyst materials. Ind Eng Chem Res 2020;59:6840–54.

[21] Mbeugang CFM, Li B, Lin D, Xie X, Wang S, Wang S, et al. Hydrogen rich syngas production from sorption enhanced gasification of cellulose in the presence of calcium oxide. Energy 2022;228:120659.

[22] Zhang C, Li Y, Yang Y, Fan X, Chu L. Analysis on H_2 production process integrated $CaO/Ca(OH)_2$ heat storage and sorption enhanced staged gasification using calcium looping. Energ Conver Manage 2022;253:115169.

[23] Fuchs J, Schmid JC, Müller S, Hofbauer H. Dual fluidized bed gasification of biomass with selective carbon dioxide removal and limestone as bed material: a review. Renew Sustain Energy Rev 2019;107:212–31.

[24] Di Giuliano A, Capone S, Anatone M, Gallucci K. Chemical looping combustion and gasification: a review and a focus on European research projects. Ind Eng Chem Res 2022;61:14403–32.

[25] Goel A, Moghaddam EM, Liu W, He C, Konttinen J. Biomass chemical looping gasification for high-quality syngas: a critical review and technological outlooks. Energ Conver Manage 2022;268:116020.

[26] Coppola A, Sattari A, Montagnaro F, Scala F, Salatino P. Performance of limestone-based sorbent for sorption-enhanced gasification in dual interconnected fluidized bed reactors. AIChE J 2023;69:e17588.

[27] Coppola A, Scala F, Gargiulo L, Salatino P. A twin-bed test reactor for characterization of calcium looping sorbents. Powder Technol 2017;316:585–91.

[28] Coppola A, Esposito A, Montagnaro F, De Tommaso G, Scala F, Salatino P. Effect of exposure to SO_2 and H_2O during the carbonation stage of fluidised bed calcium looping on the performance of sorbents of different nature. Chem Eng J 2019;377: 120626.

[29] Scala F, Montagnaro F, Salatino P. Attrition of limestone by impact loading in fluidized beds. Energy Fuels 2007;21:2566–72.

[30] Coppola A, Montagnaro F, Scala F, Salatino P. Impact fragmentation of limestone-based sorbents for calcium looping: the effect of steam and sulphur dioxide. Fuel Process Technol 2020;208:106499.

[31] Sun P, Grace JR, Lim CJ, Anthony EJ. Determination of intrinsic rate constants for the $CaO-CO_2$ reaction. Chem Eng Sci 2008;63:47–56.